and since both the distance r and the speed q are unaffected by the encounter, it follows that the areal constant is changed in proportion to the change of path angle $\delta\gamma$, i.e.,

$$\delta h/h = -(\tan\gamma)\delta\gamma \quad (3)$$

Finally the change of path angle $\delta\gamma$ is seen to be identical with the (negative of the) deflection angle Δ associated with the hyperbolic relative encounter between the mascons and the close-passing spacecraft. That the encounter orbit is relatively hyperbolic is assured by the fact that the total mass of the mascons is vastly smaller than the principal lunar mass, notwithstanding that they may be much closer to the spacecraft than the moon's center is. The deflection Δ produced by a single mascon of mass m and gravitational constant μ_m is easily found to be given by the "miss distance" l from the velocity vector of q to the mascon center, by the formula

$$\Delta = 2\frac{m}{M}\cdot\frac{a}{l}\frac{1-e^2}{1+2e\cos\theta+e^2} \quad (4)$$

when, as in the present case, the right side is numerically small compared with unity. Successive substitutions of (4), (3), and (2) into (1) then leads to the formulas for the cumulative displacements of perilune and apolune, in dimensionless form as

$$\frac{\delta r_1}{a} = -\frac{\delta r_2}{a} = 2(1-e^2)^2\frac{\sin\theta}{(1+e\cos\theta)(1+2e\cos\theta+e^2)}\times\frac{m}{M}\cdot\frac{a}{l} \quad (5)$$

where θ is the true anomaly and the path angle formula

$$\tan\gamma = e\sin\theta/[1+e\cos\theta]$$

is employed, obtainable by differentiation of the orbit equation

$$r = a(1-e^2)/[1+e\cos\theta]$$

Conclusions and Interpretations

According to Eq. (5), a single mascon of mass m and such depth as to give miss distance l when added to the distance of the spacecraft above the lunar surface, leads to observed *increase* of apolune distance, $\delta r_2 > 0$ when the mascon location is ahead of perilune (i.e., $\sin\theta < 0$). Further, both r_1 and r_2 remain constant if the apse line passes through the mascon, here treated as coplanar with the spacecraft orbit. It follows that the effects of two mascons on the opposite sides of the moon 180° apart cancel each other and that the orbit disturbances of numerous arbitrarily located mascons are minimized by maintaining near-parabolic orbits. An added measure of protection against navigational disturbances created by mascons is afforded by locating the orbital axis (line of $\theta = 0$) so as to pass through an appropriately defined center of the field of mascons. The effects of numerous mascons is in any case represented by a sum of terms like those appearing on the right side of (5).

It should be noted that J. L. Lagrange, in the third chapter of the second part of Vol. 2 of *Mécanique Analytique*, posed the identical problem to the one considered here, prefacing his analysis with the observation that the problem could have absolutely no application in the solar system. Lagrange thought of disturbing masses as necessarily having independent motions, and not solidly held within larger masses, as in the case with mascons and the moon. His analysis, characteristically ingenious and clever, does not lend itself to easy interpretation in the manner of the approximation (5), however.

Reference

[1] Muller, P. M. and Sjogren, W. L., "Mascons: Lunar Mass Concentrations," *Science*, Vol. 161, No. 3842, 1968, pp. 680–683.

Heat-Sterilizable Capsule Spin Motors

D. J. Norton*
Jet Propulsion Laboratory,
California Institute of Technology, Pasadena, Calif.

Nomenclature

F = force on the spacecraft
h = distance from nozzle to point in plume
I = moment of inertia
L = external torque
M = Mach number
P_0 = stagnation pressure
q_∞ = dynamic pressure
$\dot{q}$ = heating rate
R = radius, gas constant
r_e = nozzle exit radius
S = separation distance between capsule and spacecraft
T_B = propellant bulk temperature
T_0 = stagnation temperature
t = time
Z = distance between plane of spin motor and c.g.
α = pointing angle due to spin-up
β = nutation angle
γ = specific heat ratio
δ = total pointing angle error
η = spin motor canting angle
ϵ = nozzle expansion ratio
$\dot{\theta}_0$ = initial tip-off rate
ρ = density of gas in plume
σ = standard deviation
ϕ = relative angle between spacecraft and capsule
ω = angular velocity

Subscripts

e = nozzl exiet properties
0 = stagnation conditions

Introduction

THIS Note discusses an investigation of the use of heat-sterilized solid-propellant motors for the spin stabilization of planetary landing capsules. Figure 1 presents a

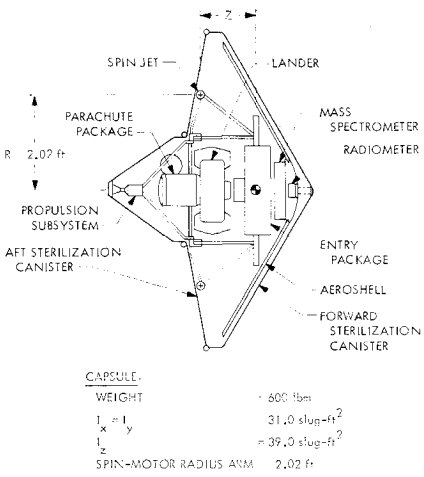

Fig. 1 Capsule configuration.

Presented as Paper 69-823 at the AIAA 5th Propulsion Joint Specialist Conference, U.S. Air Force Academy, Colo., June 9–13, 1969; submitted June 30, 1969; revision received September 15, 1969. This paper presents the result of one phase of research carried out at the Jet Propulsion Laboratory, California Institute of Technology, under Contract NAS 7-100, sponsored by NASA.

* Senior Engineer/Captain, U.S. Army Ordnance Corps, Solid Propellant Engineering Section. Member AIAA.

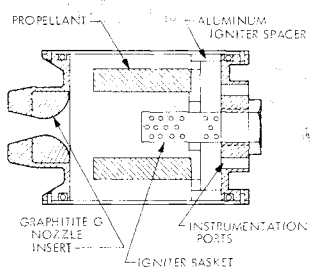

Fig. 2 Schematic of capsule spin motor.

schematic of a possible capsule assembly with the sterilization canister in place. The canister provides a sealed container within which the capsule can be heated to destroy existing microorganisms without introducing additional ones. The capsule is mated to a spacecraft which provides guidance and control, communication, and electrical power.

The capsule deflection maneuver is accomplished by a sequence of events all of which influence the total pointing error. The first step occurs as the spacecraft and capsule are separated, usually by compressed springs. This gives the capsule a velocity relative to the spacecraft and an initial tip-off rate $\dot{\theta}_0$, which is caused by nonuniformities in the spring constants and the unlatching sequence. Ideally, the spin-up of the capsule should take place immediately to prevent a buildup of error caused by the tip-off rate. However, there must be some separation distance between the capsule and the spacecraft before the spin motors are ignited to prevent unwanted forces and heating rates on the spacecraft caused by plume impingement.

The next phase of the deflection maneuver is the firing of the spin motors. It is desirable that the two motors act as a pure couple. Thus, any difference in the ignition times, thrust level, or impulse will contribute to additional pointing errors. These errors are lumped together as an angle α, with a nutation β about the new direction vector. Finally, there is the thrusting portion of the maneuver to obtain the necessary change in velocity. In this Note, only those errors associated with separation and spin-up will be considered. Thus, the spin-up pointing error can be expressed as

$$\delta = \int_0^{t_1} \dot{\theta}_0 dt + \alpha \qquad (1)$$

where t_1 = time between separation and spin-motor initiation.

Experimental Phase

Since there were no existing motors of the proper size that could be heat sterilized, a spin motor whose grain weight and geometry could be accurately controlled was designed (see Fig. 2). The hardware employed was used originally as a despin motor on a Jupiter missile re-entry nose cone program. The grain is an internal- and external-burning, cartridge-loaded cylinder. This design permits accurate machining, rapid burning of the required mass of propellant, as well as a relatively neutral pressure-time history. A short burning time is desirable to stabilize the capsule quickly.

The cantilevered charge must resist slump at the 275°F sterilization temperatures. The Aerojet formulation (AN-583-AF) selected is heat sterilizable in excess of 6 cycles at 275°F for 56 hr each, and its hardness actually increases after cycling, permitting accurate machining.

Twelve motors were fabricated, paired on the basis of charge weights and nozzle throat diameters, and heat-sterilized. They suffered a 1.5% weight loss, but the weights of the matched pairs were still within 0.1%. The results of the twelve motor firings are presented in Table 1. The most important factor for these motors is the reproducibility of matched pairs, since variation within a pair is the cause of spin-up errors. Four pairs were fired at ambient temperature (~80°F). Two pairs were fired at 160°F to determine the effect of propellant bulk temperature as it might be affected by solar radiation. Figure 3 presents typical pressure-time traces for the motors subjected to 80 and 160°F. Although P_{av} changed by 15%, $\int Pdt$ did not change appreciably. A comparison of all the firings indicates that the pressure-time integral could be kept to approximately 1% for sterilized matched pairs. The variation in the ignition times was kept below 5%. Part of this variation is believed to be attributable to the effects of sterilization on the surfaces of igniter materials, and to the charge. The 3σ, 80% confidence estimates of worst-case pair performance

Table 1 Motor firing results

Pair	T, °F	$\int Pdt$, psia-sec	$\Delta t_{ign.}$[a] msec	Δt,[b] msec	P_{av},[c] psia
1	~80	483.3	60	531	910
		478.4	62	531	901
2	~80	491.3	63	535	920
		492.2	61	532	923
3	~80	494.6	63	519	952
		492.2	61	521	945
4	~80	489.8	60	542	904
		487.5	58	546	893
5	160	486.3	55	460	1057
		487.7	58	470	1038
6[d]	160	494.8	62	457	1082
		...	62	...	...
σ, for matched pairs		0.851	0.000492	0.00188	2.295
Expected range for 3σ worst case with 80% confidence		±5.22	±0.0026	±0.0114	±14.0

[a] Δt_{ig} = time from squib current initiation to 90% of P_{max}.
[b] t_b = action time, the time between 10% of P_{max} during ignition to the same value at burnout.
[c] P_{av} = pressure derived from $\int Pdt/\Delta T$.
[d] Motor 2 of pair 6 lost its nozzle plate at normal operating pressure due to worn case pinholes.

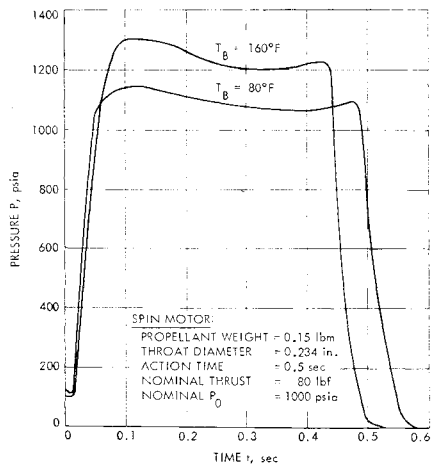

Fig. 3 Typical pressure-time histories for spin motors.

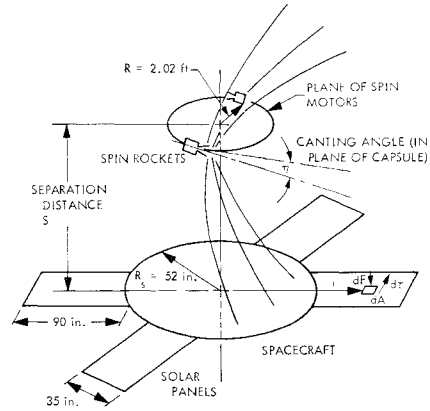

Fig. 4 Impingement of spin-motor plume on spacecraft.

Table 2 Force, torque, and heating rate tolerated by the spacecraft

Effect	Maximum total value	Maximum during 0.5-sec burn	S required, ft
Linear impulse	65 lbf-sec	130 lbf	2.0
Angular impulse	7.2 lbf-ft-sec	14.4 lbf-ft	5.0
Heat transfer	1.6 Btu/ft²	3.2 Btu/ft²-sec	4.5

were used in the analytical phase to predict pointing-angle errors caused by pair mismatch.

Plume Analysis

Forces and heating rates imposed on the spacecraft by the spin-motor plumes depend on the separation distance (Fig. 4) and were estimated as follows. The plume density distribution is assumed to be of the form[1,2]

$$\frac{\rho}{\rho_e} = \frac{E}{2}\left(\frac{V_e}{V_{\max}}\right)\left(\frac{h}{r_e}\right)^{-2}\cos(\theta)^N \tag{2}$$

where E and N are constants determined by integrating the mass and momentum equations assuming $(h/r_e) \gg 1$

$$E = \frac{1 + M_e^{-2}}{[1 + 2/(\gamma - 1)M_e^2 - (1 + 1/\gamma M_e^2)]^{1/2}} \tag{3}$$

$$N = E - 1 \tag{4}$$

It is assumed that the presence of the spacecraft in the flowfield does not alter the structure of the plume.

The equation for the pressure exerted by rebounding molecules (in free molecular flow) on the spacecraft is given by $q_\infty = 2\rho V_{\max}^2$, where $V_{\max}$ is the maximum velocity obtainable by expanding to zero pressure. This expression is conservative because it assumes a perfect, elastic collision with the spacecraft and because the maximum gas velocity is used.

The total force on the spacecraft is given by

$$F = \int q_\infty dA \tag{5}$$

Since the spin rockets are symmetrically placed around the capsule, no substantial pitch or yaw torques should be applied to the spacecraft since the tip-off angle is small ($\sim 1°$). The roll torque is given by

$$\tau = \tfrac{1}{2}\int q_\infty \cos\phi \sin\mu r dA \tag{6}$$

where ϕ is the angle of incidence, μ is the angle between the local exhaust flow direction and the radius to the element under consideration, and r is the moment arm of the area element from the roll axis. This expression is conservative in that it assumes the gas molecules are stopped by the spacecraft.

The plume impingement heating was estimated by making some conservative approximations as follows: 1) the exhaust gases are thermally and calorically perfect, 2) the flow is isentropic, 3) the exhaust gases convert all their kinetic energy into thermal energy, and 4) all of the thermal energy is absorbed by the spacecraft;

$$\frac{\dot{q}}{A} = P_0 T_0 M c_p \left[\frac{\gamma}{RT_0}\left(1 + \frac{\gamma - 1}{2}M^2\right)^{-(\gamma+1)/(\gamma-1)}\right]^{1/2} \tag{7}$$

The spacecraft was assumed to be a cruciform composed of a central disk representing the main body and four rectangular appendages representing the solar panels (Fig. 4). To calculate the effects of the spin motor plume, Eqs. (5–7) are integrated over that portion of the plume which intersects the spacecraft. The orientation of the capsule is then rotated with respect to the fixed spacecraft so that the maximum values of F, τ, and $\dot{q}$ could be obtained. The calculation was then repeated for different separation distances and expansion ratios of the nozzles.

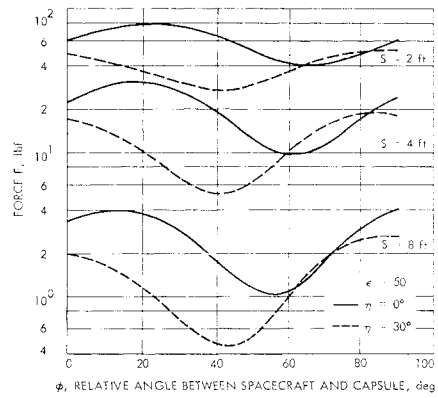

Fig. 5 Force as a function of angular position and axial separation.

Figure 5 presents the variation in the force upon the spacecraft as the capsule rotates. Because the solar panels come into view of the plume periodically, the force is a function of the relative angular position of the spacecraft to the spin motors, and it is highly dependent upon the separation distance. The dashed curves represent the force on the spacecraft when the spin motors have been canted away from the tangent to the radius of the motors (Fig. 4). This rotation of the spin motors tends to reduce the impingement while causing a small decrease in spin-up efficiency. The forces for $S = 16$ ft are $\sim 2\%$ of those for $S = 8$ ft.

Figure 6 presents the average force and torque and the maximum heating rate incident upon the spacecraft (for $\eta = 0$ and 30°), as the capsule separates. The maximum allowable linear impulse and angular impulse are determined by constants placed on the guidance of the spacecraft. For the maximum heat transfer it was determined that 1.6 Btu/ft² would increase the temperature of 5-mil aluminum sheet by 100°F. Table 2 presents typical maximum values of F, τ, and $\dot{q}$ that the spacecraft can tolerate, along with the corresponding separation distances from this analysis. The $\dot{q}$ and τ required the greatest separation distance. It must be emphasized that these calculations are conservative.

Pointing Error Analysis

To complete the spin-up pointing error α, the equations of motion for rigid-body dynamics were programed.[3,4] The

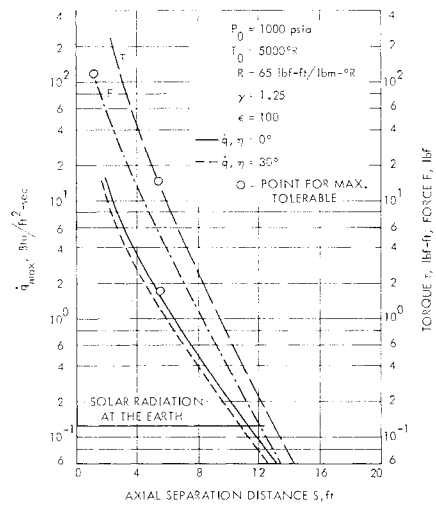

Fig. 6 Average torque τ and force F and maximum heating rate $\dot{q}_{\max}$ vs axial separation distance.

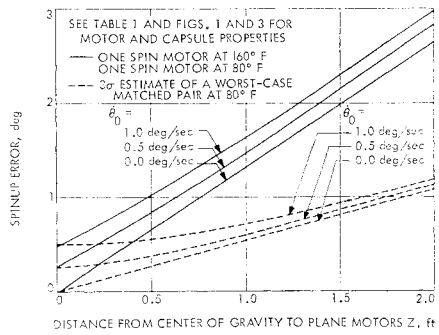

Fig. 7 Results of calculations for pointing error caused by spin-up.

3σ estimates of worst-case spin-motor mismatch (Table 1) were then employed to generate simulated pressure-time curves which served as the forcing function for the motion of the capsule. Since the spin motors weighed approximately 1 lb, as compared to a capsule weight of 600 lb, the assumption of constant mass simplified the governing equations as follows:

$$I_x\dot{\omega}_x - (I_y - I_z)\omega_y\omega_z = L_x \quad (8)$$

$$I_y\dot{\omega}_y - (I_z - I_x)\omega_x\omega_z = L_y \quad (9)$$

$$I_z\dot{\omega}_z - (I_z - I_y)\omega_x\omega_y = L_z \quad (10)$$

where $L_x = F_1(t)R_1 - F_2(t)R_2$, and $F(t)$ = the thrust time function for spin motor (1 or 2). The angular velocities were determined by simultaneous integration of these equations from the following initial conditions: $(\omega_{x0}^2 + \omega_{y0}^2)^{1/2}$ = tip-off rate = $\dot{\theta}_0$, and ω_{z0} = roll rate = 0. After determining the angular velocities, the angular position of the capsule was determined as a function of time.

Thus, differences in Δt_i, t_b, and P_{av} were investigated by calculating α, for a 3σ estimate of spin motor mismatch as a function of Z, and $\dot{\theta}_0$. When the spin motors are coplanar and $\dot{\theta}_0 = 0$, there is no effect of spin-motor mismatch. This determines the optimum location of the spin motors. Figure 7 presents the results of a number of calculations for pointing error caused by spin-up. The dependence upon $\dot{\theta}_0$ becomes relatively less important as Z increases. As Z increases the differences in the spin motors are accentuated. When one motor was heated to 160°F, the change in burning rate (Fig. 3) caused increases in α even though $\int Pdt$ of the two motors was the same. This is attributable to shift in magnitude and time sequence of thrust of the motors.

Conclusions

A propellant (Aerojet AN-583-AF) has been demonstrated which provides a high-modulus, heat-sterilizable formulation useful in accurate machining of highly reproducible charges. The sterilized spin-motor firings indicate that differences in total impulse and average pressure can be maintained at or below the 1% level.

To minimize the spin-up pointing error for given spin motors, Z and $\dot{\theta}_0$ should be kept to a minimum. Significant increases in pointing error results from unequal motor temperatures even if total impulses are the same. For the geometry under consideration, increasing ϵ and η do not significantly reduce the plume impingement effects.

References

[1] Karydas, A. I. and Kato, M. T., "An Approximate Method for Calculating the Flow Field of a Rocket Exhausting into a Vacuum," Publication U-2630, June 1965, Aeronutronic Div. of Ford and Philco.

[2] Kelley, J. H. and Young, D. L., interdepartmental communication, Dec. 30, 1965, Propulsion Div., Jet Propulsion Lab.

[3] Armstrong, R. S., "Errors Associated with Spinning-Up and Thrusting Symmetric Rigid Bodies," TR 32-644, Feb. 1965, Jet Propulsion Lab., Pasadena, Calif.

[4] Dobrotin, B., privatec ommunication, June 1968, Rigid Body Spin-up Computer Program, Jet Propulsion Lab.

Streamlining Vehicles for High-Altitude Hypersonic Flight

JOHN WEBSTER ELLINWOOD*
The Aerospace Corporation, El Segundo, Calif.

Nomenclature

C = Chapman-Rubesin constant; $C = [\mu(T_r)/\mu_\infty](T_\infty/T_r)$
C_D = drag coefficient based on frontal area
$C_D{}^{fm}$ = free-molecule drag coefficient
d = $C_D{}^{fm}/C_D(\bar{v}_m,\theta)$
I = integral given by Eq. (1) and Eq. (3)
N = exponent of power-law C_D given by Eq. (2)
M_∞ = freestream Mach number
R = log $(\rho_{\max}/\rho)$
$Re_{\infty,L}$ = Reynolds number based on freestream conditions and vehicle length
T_r = reference temperature, $T_r \approx \langle T_w, T_0/4\rangle$
T_w, T_0 = surface and stagnation temperatures, respectively
$\bar{v}$ = $M_\infty(C/Re_{\infty,L})^{1/2}$
$\bar{v}_m$ = minimum $\bar{v}$
θ = cone half angle
θ_m = θ for minimum $C_D(\bar{v}_m)$
μ = air viscosity

Introduction

THE aerodynamic designer often desires to construct a vehicle with minimum drag at some flight condition. For hypersonic flight, if the altitude of interest corresponds to free-molecule flow (above about 65 naut miles for a vehicle 30 ft long) it is well known that streamlining, in the sense of increasing the length for given frontal area, does not reduce drag. The free-molecule drag coefficient $C_D{}^{fm}$, based on frontal area, is independent of shape as long as the typical body slope θ is much larger than the reciprocal speed ratio. On the other hand, for low altitudes, where the viscous boundary layer on the vehicle is thinner than the vehicle, C_D varies as θ^2, and streamlining is aerodynamically useful.

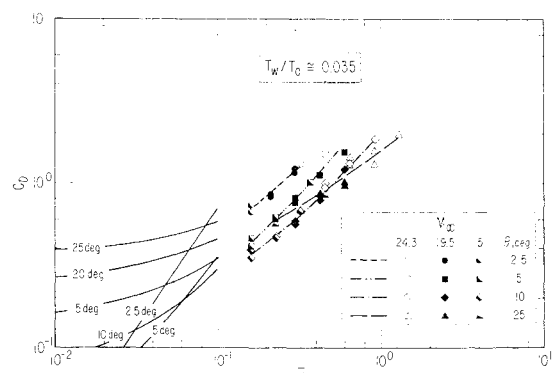

Fig. 1 Zero-lift drag coefficient of pointed cones at high altitudes.

Received June 27, 1969; revision received September 26, 1969. This work was supported by the U.S. Air Force under Contract F04701-68-C-0200.

* Member of the Technical Staff, Aerodynamics and Propulsion Research Laboratory. Member AIAA.